Influence of temperature on oxygen permeation through ion transport membrane to feed a biomass gasifier

2015 J. Phys.: Conf. Ser. 655 012034

(http://iopscience.iop.org/1742-6596/655/1/012034)

Journal of Physics: Conference Series **655** (2015) 012034 doi:10.1088/1742-6596/655/1/012034

Influence of temperature on oxygen permeation through ion transport membrane to feed a biomass gasifier

T Antonini[1] **, P U Foscolo**[1] **, K Gallucci**[1] **, and S Stendardo**[2]
[1] Industrial Engineering Department, University of L'Aquila, Via G. Gronchi, 18-67100 L'Aquila, Italy
[2] ENEA, Casaccia Research Centre, 00100 Roma, Italy

E-mail: tania.antonini@graduate.univaq.it

Abstract. Oxygen-permeable perovskite membranes with mixed ionic-electronic conducting properties can play an important role in the high temperature separation of oxygen from air. A detailed design of a membrane test module is presented, useful to test mechanical resistance and structural stability of $Ba_{0.5}Sr_{0.5}Co_{0.8}Fe_{0.2}O_{3-\delta}$ (BSCF) capillary membrane in the reactor environment. Preliminary experimental results of membrane permeation tests highlight the positive effect of temperature on perovskite materials. This behaviour is also confirmed by a computational model of *char* combustion with oxygen permeated through the membrane module, when it is placed inside a gasifier reactor to provide the necessary input of heat to the gasification endothermic process. The results show that the temperature affects the oxygen permeation of the BSCF membrane remarkably.

1. Introduction

Solid fuel (biomass, coal) gasification-based energy systems offer a reliable, affordable conversion process into fuel gas, with high-efficiency and flexibility in the production of power, heat and a wide range of chemical substances.

Building on current state of the art, gasification-based technologies can be refined and improved via application of advanced gas separation technologies that are being developed [1,2].

Most of the current commercial gasification projects, as well as those planned for the future, consider oxygen-blown gasifiers and require large flow rates of oxygen to establish auto-thermal process conditions. Thus, air separation represents a major area of opportunity for both cost reduction and performance improvement, making it a key part of energy systems. Any technology that can offer a significant reduction in the cost of oxygen will have a substantial impact on the overall economics of gasification-based processes.

Oxygen permeation through ion transport membranes is a novel technology that can be used as a replacement of energy-demanding cryogenic distillation or Pressure Swing Adsorption (PSA)/Pressure Vacuum Swing Adsorption (PVSA) processes. Cryogenic process is expensive and energy intensive, because it operates at very low temperature and at elevated pressures [3], therefore is suitable for very large plants only. In small to medium scale applications PSA or PVSA require compression of a volumetric gaseous stream at least 5 times greater than the oxygen stream effectively utilized in the gasification process with a substantial penalty of the whole energy efficiency.

Ion Transport Membranes (ITM) offer a sound alternative to conventional processes, where the goal is to provide oxygen at high temperature conditions (850-1000°C) in small to medium scale applications.

A considerable number of research works have demonstrated that dense perovskite membranes at elevated temperatures exhibit substantial oxygen ion permeability [4-9].
Ceramic dense membranes must be defect free and gas tight to hinder the gas permeation through pores, only allowing the oxygen ionic transport.
These membranes deliver oxygen ions from the feed side to the permeate side without the aid of any external electric circuit (counter diffusion of electrons preserves the electro-neutrality), which makes the process simple and very attractive.
The driving force is the difference in oxygen partial pressure across the membrane [6], so that it is not needed to pressurize the air feeding stream.
In this paper, the influence of temperature is investigated on the oxygen flux to a biomass fluidized bed gasifier equipped with an ITM module, by means of a simulation model, purposely developed to evaluate partial combustion of *char* with oxygen permeated through a tubular membrane.
In addition, a laboratory test rig has been designed, realized and is presently under operation to investigate experimentally oxygen permeation as a function of temperature exhibited by commercially available capillary membranes [7]. This study will also help identifying technological problems related to the assembly of the oxygen permeating membrane in a self standing module that could be inserted and operated in a gasification reactor.

2. Materials

Dense perovskite membranes exhibit ion permeability at elevated temperatures when subjected to a gradient of oxygen chemical potential [6]. This oxygen semi-permeability is generally attributed to the partial substitution of both A e B cations (in this study A = Ba, Sr and B = Co, Fe) in the perovskite lattice structure $(Ba,Sr)(Co,Fe)O_3$ [8, 9] and the formation of oxygen vacancies.
Their orthorhombic structure makes perovskite materials very stable at high temperature. However, the perovskite itself does not show the capability to conduct oxygen ions; there must be a certain amount of imperfections or atomic defects produced due to the non-stoichiometry of the perovskite materials.
These positively charged vacancies can be disordered at high temperature [10] and are considered to be the most mobile ionic species in these materials [11-13]. The transport of electric charges is compensated by the transport of electron-holes in the reverse direction.
Following Teraoka et al.'s work [8, 9], experimental measurements of oxygen fluxes conducted by Xu and Thomson [6] allowed to conclude that the oxygen permeation at low temperatures (750 °C) is limited by the rate of oxygen-ion recombination but is dominantly controlled by bulk diffusion at high temperatures (> 800 °C).
The cubic perovskite $Ba_{0.5}Sr_{0.5}Co_{0.8}Fe_{0.2}O_{3-\delta}$ (BSCF) is the state of the art ceramic membrane material for oxygen separation technologies above 800 °C making them most interesting for application in the gasification systems. BSCF membranes exhibit one of the highest oxygen permeabilities reported so far for dense oxides combined with excellent phase stability.
The overall oxygen flux is described by the following equation proposed by Tan and Li [14], who adapted to the case of tubular membranes the oxygen transport model originally proposed by Xu and Thomson for flat membranes [6]:

$$J_{O2} = \frac{\left[k_r \cdot \left(P_{O2}^{I\,0.5} - P_{O2}^{II\,0.5}\right)\right]}{\left[\frac{2 \cdot t \cdot k_f}{D_V}(P_{O2}^{I} \cdot P_{O2}^{II})^{0.5} + \frac{d_m}{d_{io}} \cdot (P_{O2}^{II})^{0.5} + \frac{d_m}{d_o} \cdot (P_{O2}^{I})^{0.5}\right]} \quad (1)$$

where P_{O2}^{I} and P_{O2}^{II} are the oxygen partial pressures at the membrane surface, on the feeding-side and on the permeate-side, respectively.
Each of the parameters in the above equation (D_V, k_r and k_f) is expressed as a function of the membrane temperature, T_w, by means of an Arrhenius type equation. Pre-exponential factor and

activation energy values were reported by Xu and Thomson [6] by fitting experimental data of oxygen permeation rates through LSCF ($La_{0.6}Sr_{0.4}Co_{0.2}Fe_{0.8}O_{3-\delta}$) ion-conducting membranes.
More recently, oxygen permeation properties were investigated using a high temperature permeation setup at TU/e (Technical University of Eindhoven, Nederland) [15,16]; two BSCF tubular membranes produced by VITO, with different thickness, were tested. Their specifications are listed in Table 1, together with corresponding parameters characterizing the membrane samples adopted in this study.
Two basic parameters affect positively the oxygen permeation flux: temperature and oxygen partial pressure on the permeate side. High temperature systems improve oxygen permeation rate because of the Arrhenius type dependence law of the parameters D_V, k_r and k_f. On the other hand, by increasing the sweep gas flow rate on the permeate side, the oxygen pressure decreases, as a consequence the driving force across the membrane increases with an improvement in the oxygen permeation flux.

Table 1. Chemical and geometric characteristics of membranes tested at TU/e [15] and in this study.

University	Composition	Acronym	Length [mm]	Outer Diameter [mm]	Thickness [mm]
TU/e	$Ba_{0.5}Sr_{0.5}Co_{0.8}Fe_{0.2}O_{3-}$	$BSCF_{(1)}$	100	2.7	0.20
TU/e	$Ba_{0.5}Sr_{0.5}Co_{0.8}Fe_{0.2}O_{3-}$	$BSCF_{(2)}$	100	3.5	0.50
This study	$Ba_{0.5}Sr_{0.5}Co_{0.8}Fe_{0.2}O_{3-}$	$BSCF_{(3)}$	60	3.5	0.35

A MATLAB® routine was developed to solve a non linear least-squares regression model applied to the permeation data (oxygen fluxes) obtained with the newly developed membranes [1, 15]. In the equation (1) of the oxygen permeation flux, the bulk diffusion coefficient, D_V, and the forward surface exchange rate constant, k_f, appear as their ratio and the contribution of this term is relatively small when compared to the remaining terms. In addition, k_r is a multiplying factor of the whole expression of the oxygen flux. For these reasons, in the regression model k_f and D_V have been maintained those suggested by Tan and Li [14], whereas the pre-exponential factor and the activation energy of k_r have been determined, those minimizing the difference between calculated and experimental values.
As shown in Table 2, it is worth noticing a substantial reduction in the k_r activation energy that is halved compared to the respective value proposed by the previous model [6], confirming that these newly developed membranes are activated at relatively lower temperatures.
In Figure 1, experimental measurements done at TU/e and model predictions of oxygen fluxes are compared in a parity plot: an excellent match is obtained.

Table 2. Pre-exponential factor and activation energy of the parameters in equation (1): values proposed by Xu and Thomson [6] and (last row) the modified k_r according to the state of the art permeation data.

Parameter	Pre-exponential factor	Activation Energy, E_A [kJ/mol]
D_V [cm^2/s]	$1.58 \cdot 10^{-2}$	73.6
k_f [$cm/atm^{0.5}/s$]	$5.90 \cdot 10^{6}$	226.8
k_r [$mol/cm^2/s$]	$2.07 \cdot 10^{4}$	241.3
k_r [$mol/cm^2/s$] (state of the art)	3.33	122.0

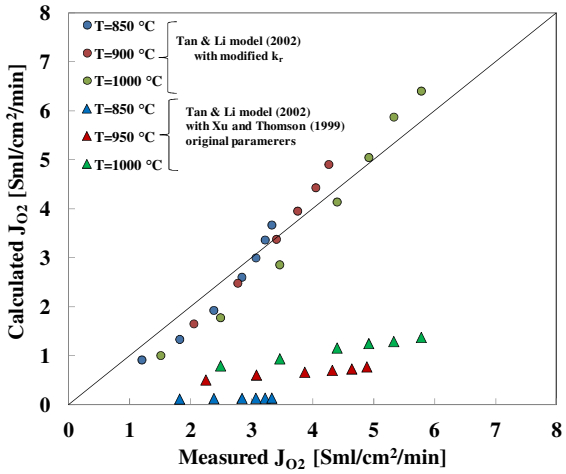

Figure 1. Parity plot of measured vs. calculated O_2 permeability through VITO BSCF tubular membranes, at different temperatures; predictions are performed with the Xu and Thomson model [6] utilizing the original D_V and k_f parameter values and k_r proposed in [1, 15] (Table 2), respectively.

3. Test module to measure oxygen permeation fluxes

Oxygen permeability and structural stability are two key factors of MIEC (Mixed Ionic Electronic Conducting) materials. Generally, material stability is opposite to the oxygen flux value.

In order to seek the tradeoff between the two factors according to the requirements of the environment for a specific application, the design of a module for oxygen generation with a BSCF membrane has been developed.

There are different schools of thought to connect the membrane with the test module.

Fixed-ends configurations, although widely suggested in literature [16] resulted inadequate, causing membranes to break during heat treatment because of different thermal expansion of the perovskite material and the remaining alumina and steel pipes of the reactor module. Instead, a suitable reactor layout is a *once-through* configuration, to reduce thermal stresses by allowing differential dilatation of materials during heating cycles.

An additional goal pursued in this research activity was to minimize the junctions placed inside the hot furnace, limiting them to those involving the membrane itself. The steel/alumina connections to arrange the input of the feeding stream and the output of the permeate stream were located outside the hot region and stainless steel pipes have been used, connected by means of standard SWAGELOK ® junctions. Figure 2 illustrates the whole layout.

The most critical point in assembling the test module is sealing the perovskite capillary membrane to the alumina pipes for adduction and withdrawal of gaseous streams.

The sealing system has been widely studied at TU/e [16], therefore in this work the same technique will be adopted in assembling the membrane reactor.

The inlet gas, helium, see Figure 2, is fed from the bottom of a 99.7% Al_2O_3 capillary (4) placed inside two co-axial 99.7 % Al_2O_3 pipes (1) and (5), where the capillary membrane (3) is housed. Air, at room conditions, flows between the electric furnace inside wall and the membrane outside surface. The test module is shown in Figure 2b and its components are listed in Table 3.

The first step in assembling the module (see Figure 2) is to fix the inner (600 mm long) and outer (400 mm long) Al_2O_3 tubes with silicone adhesive in their respective stainless steel holders (6) and (8), as shown in Figure 3A – 3B.

With reference to Figure 2, the perovskite capillary membrane was connected to alumina pipes by a suitable high temperature gas-tight sealant. Both edges of the membrane surface are protected from chemical reactions by spreading MaTeck gold conducting paste on a capillary segment about 1 cm deep, on each side, see Figure 3C.

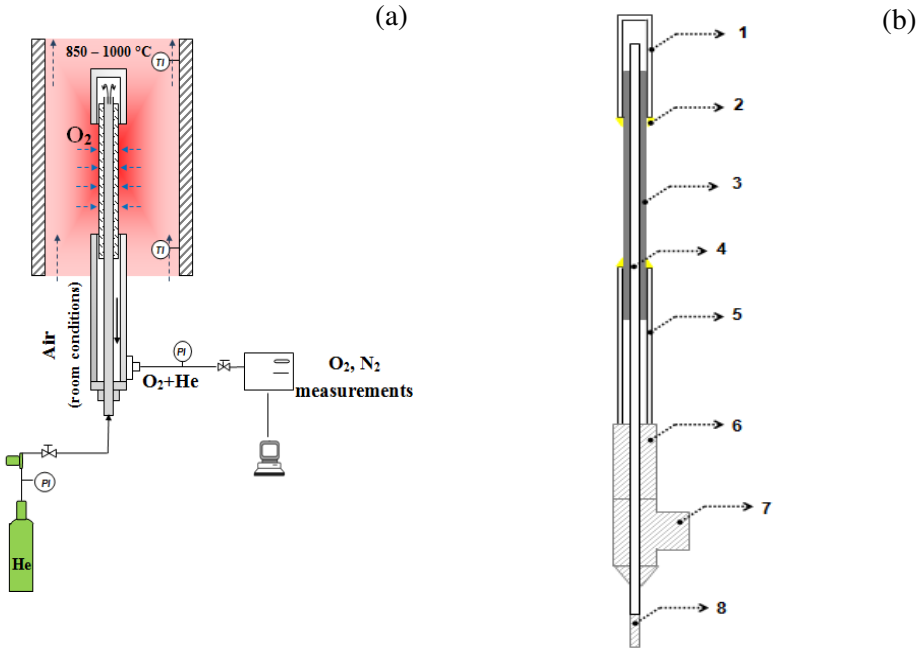

Figure 2. a) Test rig for high temperature oxygen permeation measurements; b) detailed view of the membrane module (components are listed in Table 3).

Table 3. Components of BSCF capillary test module (reference is made to Figure 2b).

1	Al_2O_3 cup (L_1=20 mm, OD_1=6 mm, ID_1=4 mm)
2	Sealing system (gold paste + glass seal)
3	BSCF capillary membrane (as in Table 1)
4	Inner Al_2O_3 tube (L_4=600 mm, OD_4=1.6 mm, ID_4=1 mm)
5	Outer Al_2O_3 tube (L_5=400 mm, OD_5=6 mm, ID_5=4 mm)
6	Stainless steel fitting (Al_2O_3 outer pipe holder)
7	"Tee" tube fitting (permeate output flow, O_2 in He)
8	Stainless steel fitting (He input flow)

The gold paste was dried for 1 h at room temperature and then placed in an oven for the curing procedure (heated up to 1000 °C at a rate of 2 °C/min, kept for 1 h at the maximum temperature, then cooled down to room temperature). The second step consisted of applying the glass seal (Schott 8252) on top of the gold paste, Figure 3D, inserting both membrane heads into the alumina pipes and sealing the joints by heating the sample to 1020 °C at a rate of 2 °C/min, holding it for 1 h at the maximum temperature level and cooling it down to the desired operating temperature (about 850 °C). Gas leaks were monitored by measuring the concentration of nitrogen on the permeate side (by GC analysis).

3.1 Estimated high temperature oxygen permeation fluxes

Preliminary permeability tests were carried out in the range of temperature 850 – 950 °C; the helium flow rate on the sweep side was varied from 80 to 350 Sml/min in order to investigate the influence of the O_2 partial pressure in the permeate. During the experimental campaign, a maximum heating rate of 2 °C/min was used to prevent the sealing and the membrane from cracking due to thermal stresses and

the temperature level was always kept above 800 °C. The oxygen permeation flux estimated from the experimental measurements is reported in Figure 4 as a function of temperature, at different He flow rates.

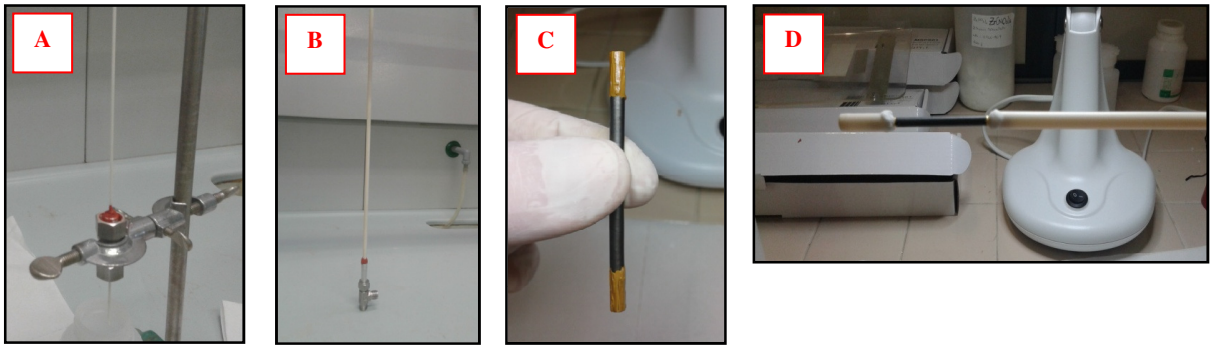

Figure 3. Assembling sequence of the test module for high temperature oxygen permeation measurements: sealing the inner (A) and outer (B) Al_2O_3 tubes in their respective stainless steel holder, (C) MaTeck gold conducting paste at the end of the BSCF capillary, (D) sealing the membrane with the Schott glass paste between the Al_2O_3 cup and the outer tube

The permeation fluxes obtained in this study (Figure 4b) are compared with the corresponding data obtained at TU/e in the experimental study mentioned above [15] (Figure 4a). The permeability shown in Figure 4b is somewhat higher than that in Figure 4a, although of the same order of magnitude; this result can be partially ascribed to the reduced thickness of the membrane employed in this study (Table 1). According to the Arrhenius type dependence law, O_2 permeation rates increase considerably with increasing temperature. A positive effect on the O_2 flux values is also found increasing the sweep gas flow rate, He, because the oxygen partial pressure on the permeate side decreases.

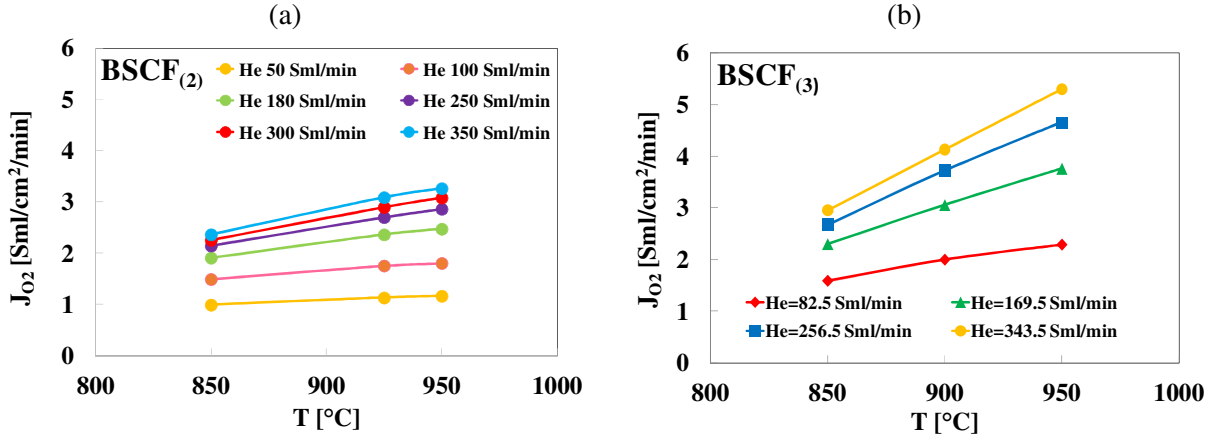

Figure 4. O_2 permeation fluxes as a function of temperature obtained at TU/e (a) and in this study (b) with the BSCF membrane specifications reported in Table 1.

In the experimental procedure, gas samples were analyzed by gas chromatography using a Thermal Conductivity Detector (TCD) and helium as gas carrier (its flow rate is fixed at 20 ml/min). The calibration curve is obtained by performing GC analysis of three standard gas mixtures (1% O_2 - 4% N_2 in He, 10% O_2 - 40% N_2 in He and 30% O_2 - 50% N_2 in He): the relative surface area of peaks is used in the calculations with the unknown gas samples collected during the experiments.

4. Computational model of ITM oxygen permeation in a biomass gasifier

In a previous work [1], a new concept for integration of gasification with oxygen transport membranes and hot gas cleaning in one reactor vessel has been developed in order to obtain a clean fuel gas from

biomass that would allow immediate and efficient conversion into power (high temperature fuel cells, gas turbines, bio-fuels or chemicals). A simplified schematization of that concept is illustrated in Figure 5.

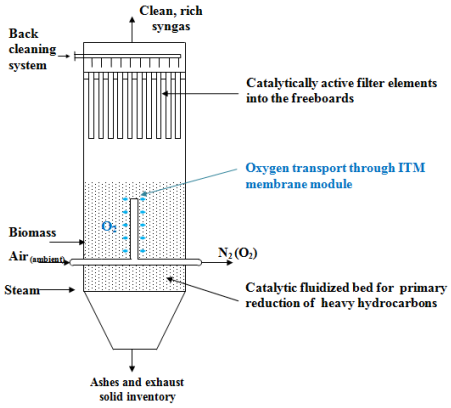

Figure 5. Integration of gasification with ITM membrane module.

In order to investigate the influence of temperature on oxygen permeation flux, numerical evaluations are performed for a single ITM capillary membrane, with the specifications summarized in Table 3, immersed vertically inside the fluidized bed where particles are considered uniformly dispersed in the bed layer surrounding the membrane module and air (oxygen 21% by volume) at atmospheric pressure flows inside the membrane; the air superficial velocity inside the ITM module is fixed (u_{in} = 5 m/s).
In small to medium scale applications (up to 10 MW_{th}) , the knowledge of the gasifier total oxygen demand allows to fix the inlet air flow rate, Q_{air}, and the oxygen transfer system configuration:

$$Q_{air}\frac{P}{R\,T}\left(y_{O_{2,in}} - y_{O_{2,out}}\right) = J_{O_2} A_m N \left(1 - y_{O_{2,out}}\right) \tag{2}$$

where the oxygen depletion in the outlet stream $y_{O_{2,out}}$ is kept above a fixed limiting value,
The oxygen demand to assure autothermal behavior of a pilot scale biomass gasifier is of the order of 10 moles per kg of biomass (about 25% of what would be needed for complete combustion); so with a biomass feedstock of 200 kg/h (corresponding to a gasifer capacity of 1 MW_{th}) the oxygen demand would be of the order of 2 kmol/h and the membrane surface area of about 18 m^2, with an expected oxygen permeation flux of 3 µmol/cm^2/s. The required number of BSCF membrane pipes can be easily arranged inside the gasifier vessel, considering both a reactor inner diameter of the order of 0.3 - 0.5 m. and a reactor height of the order of 4 - 5 m. The membrane bundle configuration could be chosen so to assure optimum oxygen distribution within the reactor; membrane pipes with greater diameter could be also adopted to reduce their number. The *char* fraction inside the fluidized bed is fixed to be on average w_c = 6 % by weight, according to the gasification results reported in [17].

4.1 Description of model equations

In what follows, reference is made to oxygen transfer to the fluidized bed and its consumption by means of *char* combustion: an heterogeneous reaction process. Once the expected oxygen permeation flux is fixed, the geometric specifications of the ITM system are obtained:

$$A_m = \pi \cdot d_m \cdot L, \qquad d_m = \frac{2 \cdot t}{ln[(d_o)/d_{io}]} \tag{3}$$

where t is the membrane thickness, d_o and d_{io} are the perovskite membrane outside and inside diameters, respectively.
Local steady state conditions are imposed; knowing from previous works [18, 1] that the resistance on the air side is negligible allows to disregard it. Two oxygen transfer resistances in series are therefore

considered: the former in the perovskite membrane, the latter related to oxygen mass transfer in the fluidized bed, enhanced by simultaneous *char* combustion.
The combustion process of small *char* particles in the fluidized bed is relatively fast, so that the depth of penetration of the concentration and temperature perturbation is expected very thin in comparison with the fluidized bed scale, of the order of a few millimetres. As a result, a one-dimensional analysis in the tubular membrane radial coordinate is appropriate and resistance to mass and energy transport are assumed to take place in a gaseous layer at the inter-phase transfer surface (sweep side).
The global combustion reaction rate, $\mathbf{r_c}$ (*char* moles burnt per unit time and fluidized bed volume) is assumed to depend linearly on the local oxygen concentration [19]:

$$\boldsymbol{r_c} = k_O \cdot C_{O2}; \qquad 1/k_O = 1/(k_c \cdot a_c) + 1/\left(k \cdot \rho_{M,c}/\rho_{M,g}\right) \tag{4}$$

A diffusion-controlled combustion regime is established because the mass transfer rate constant is small compared to the reaction rate constant at the high temperature level in the gasifier.
If *char* is considered to be pure carbon, the reaction stoichiometry can be expressed as follows:

$$C + \delta O_2 \rightarrow 2(1-\delta)CO + (2\delta - 1)CO_2 \tag{5}$$

where the value of δ is estimated from Arthur empirical correlation [20] as a function of temperature.
The condition of zero oxygen accumulation at the membrane/fluidized bed interface results in the following relation expressing the equality between the oxygen flow transported through the membrane and that diffusing toward the fluidized bed:

$$J_{O_2} \cdot d_m = -\rho_{M,gas} \cdot D^e_{O_2} \cdot \left(\frac{dy_{O_2}}{dr}\right) \cdot 2\,r \;\; at\; r = d_o/2 \tag{6}$$

In order to evaluate the derivative on the RHS of the above equation, the oxygen concentration profile should be obtained by integration of the differential, stationary mol balance in the fluidized bed layer adjacent to the membrane pipe:

$$\rho_{M,gas} \cdot D^e_{O_2} \cdot \frac{d}{dr} \cdot \left[r \cdot \left(\frac{dy_{O_2}}{dr}\right)\right] = \delta \cdot r \cdot \boldsymbol{r_c} \tag{7}$$

The product $\rho_{M,gas} \cdot D^e_{O_2}$ can be reasonably considered constant in this study because temperature fluctuates no more than 5% of its absolute value in the fluidized bed, T_B, as it will be shown later.
Boundary conditions:

$$r = \frac{d_o}{2} \rightarrow y_{O_2} = P^{II}_{O_2}/P \qquad r = \infty \rightarrow y_{O_2} = y_{O_2,bulk} = 0 \tag{8}$$

The above equations (1) and (6) allow to determine the oxygen flux, J_{O2}, and the oxygen partial pressure on the sweep side, P_{O2}^{II} under isothermal conditions.
To estimate the importance of temperature perturbation due to the *char* combustion process, an energy balance is coupled with the oxygen molar balance.
The combustion of *char* should in principle determine a temperature increase in the fluidized bed close to the membrane surface, resulting in a membrane temperature value, T_w, above that in the bulk of the bed and in turn improving the oxygen permeation rate, due to the Arrhenius-type dependence of the parameters in equation (1). In Figure 7 both these effects are illustrated with reference to the case of study examined here.
By considering the effective thermal conductivity of *char* particles, the energy balance is expressed by the following differential equation:

$${k_t}^e \cdot \frac{d}{dr} \cdot \left[r \cdot \left(\frac{dT}{dr}\right)\right] = \Delta H_r \cdot r \cdot \boldsymbol{r_c} \tag{9}$$

Boundary conditions:

$$r = d_o/2 \rightarrow \frac{dT}{dr} = \frac{h_g \cdot (T_w - T_a) \cdot d_{io}}{{k_t}^e \cdot d_o} \qquad r = \infty \rightarrow T = T_B \tag{10}$$

At the membrane boundary, it is imposed that the heat transfer rate from the fluidized bed to the membrane should be equal to that from the membrane to the air stream. On the other hand, with reference to the boundary condition in the bulk of the gasifier, in the numerical integration it has in

fact been assumed that temperature reaches the value T_B at a distance from the membrane corresponding to complete consumption of oxygen. As a matter of fact, fluidized beds are characterized by a strong tendency to smooth temperature differences, over distances comparable with the thickness of one particle layer, as soon as the causing perturbation extinguishes [21].
To estimate the importance of this thermal perturbation quantitatively (Figure 7), it is assumed that the temperature in the bulk of the air stream on the feeding side, T_a, the fluidized bed temperature, T_B, and that of the membrane, T_w, are uniform along the membrane, and the steady state energy balance through the fluidized bed layer surrounding the whole membrane pipe is considered, coupled with the oxygen molar balance corresponding to the oxygen partial pressure at the air inlet section. The contribution of radiative heat transfer is neglected in equation (9) [22].
The system of equations (7) and (9) with corresponding boundary conditions are integrated and iterations are made till the membrane temperature, T_w, assumes a steady value that satisfies both, oxygen transfer and heat transfer constraints.

4.2 Results and discussion
The model described above was implemented in MATLAB®, and calculations were performed with reference to the membrane geometry illustrated in Figure 2b.

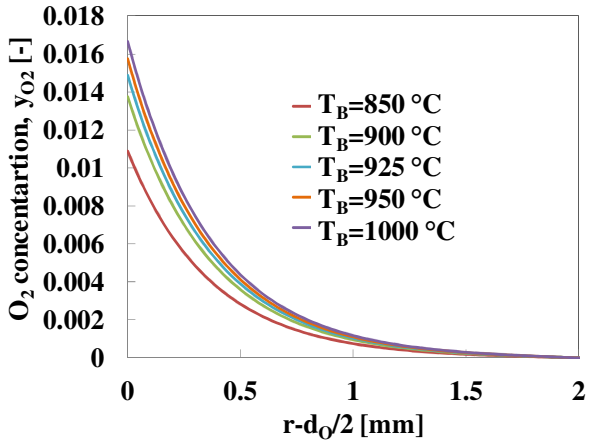

Figure 6. Calculated O_2 concentration in the fluidized bed as a function of the radial distance from the membrane surface in the range of bed temperature 850-1000 °C (w_c=6 %).

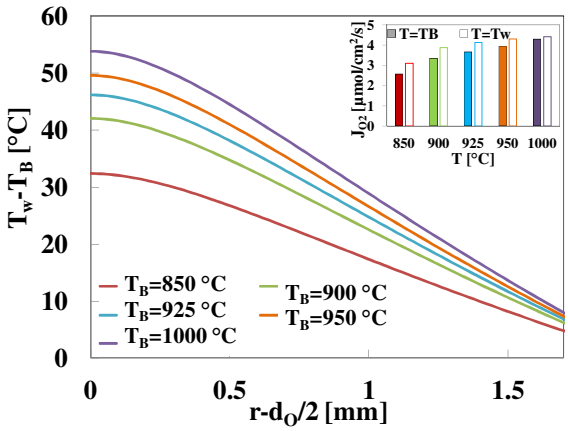

Figure 7. Calculated temperature profile as a function of the radial distance from the membrane surface in the range of bed temperature 850-1000 °C. In the insert, effect of membrane temperature increase on the O_2 permeation flux: comparison at $T=T_B$ (bed temperature) (shaded bar) and $T=T_W$ (membrane temperature) (open bar), respectively (w_c=6 %).

Figure 6 shows the oxygen molar fraction in the fluidized bed as a function of the radial distance from the membrane outer surface, with reference to the air inlet horizontal section of the membrane pipe (z = 0). It is confirmed that the O_2 concentration in the fluidized bed becomes negligible at a distance equal to or less than the membrane external diameter (d_O = 3.5 mm): the greater the *char* concentration, the steeper is the O_2 concentration profile, because the combustion reaction rate is faster.
Finally, Figure 7 allows to estimate quantitatively the temperature perturbation brought about by the exothermic *char* combustion reaction with an appreciable improvement of the membrane permeability. Temperature is imposed to approach the value T_B at a distance of about 1.7 mm from the membrane outer surface corresponding to complete consumption of oxygen, as shown in Figure 6. At T_w= 1054 °C the highest oxygen permeation rate is obtained, J_{O2}=4.4 µmol/cm^2/s.

5. Conclusions

Ion transport membranes integrated in the gasification environment are suitable to separate oxygen from air and feed it to the reactor in order to provide the necessary energy input for the autothermal gasification process, by means of combustion reactions.

Newly developed BSCF-type membranes have been tested to check the influence of temperature and sweeping gas flow rate on the oxygen permeation rates. The values observed are higher than those reported in [6] and slightly above those recently obtained at TU/e [15], with a different lab rig and measurement technique. The expected trends with membrane temperature and sweeping gas flow rate, respectively, have been validated experimentally.

The positive effect of temperature is also confirmed by the computational model. Satisfactory oxygen permeation fluxes are predicted, enough to house the whole membrane module inside the gasifier. The permeability increase due to the exothermic *char* combustion process at the membrane surface is substantial.

Finally, a test module for high temperature oxygen permeation measurements has been realized, which allows to test ITM mechanical resistance, durability and stability in inert and reactive environment.

6. Acknowledgments

The financial support from Italian National Agency for New Technologies, Energy and Sustainable Economic Development (ENEA) to this research activity is acknowledged.

7. References

[1] Antonini T, Gallucci K, Anzoletti V, Stendardo S, Foscolo P U 2014 *Chem. Eng. Process.* doi:10.1016/j.cep.2014.11.009
[2] Heidenreich S, Foscolo P U 2015 *Prog. Energy Combust. Sci.* **46** 72-95
[3] Leo A, Liu S, Diniz Da Costa J C 2009 *Int. J. Greenh. Gas Control* **3** 357-397
[4] Steele B C H 1992 *Mater. Sci. Eng. B* **13** 79-87.
[5] Bouwmeester H J M., Kruidhof H, Burggraaf A J 1994 *Solid State Ionics* **72** 185-194.
[6] Xu S J, Thomson W J 1999 *Chem. Eng. Sci*. **54** 3839–50.
[7] VITO (Vision on technology), Catalogue Materials Technology, www.vito.be.
[8] Teraoka Y, Zhang H M, Furukawa S, Yamazoe N 1985 *Chem. Lett.* 1743-1746.
[9] Teraoka Y, Zhang H M, Okamoto K, Yamazoe N 1988 *Mat. Res. Bull.* **23** 51-58.
[10] Kruidhof H, Bouwmeester H J M, van Doorn R H J E, Burggraaf A J 1993 *Solid State Ionics* **63 (65)** 816-822.
[11] Schaffrin C 1976 *Phys. Status Solidi A* **35** 79-88
[12] Baiatu T, Waser R, Hardtl K H 1990 *J. Am. Ceram. Soc.* **73** 1663-1673.
[13] Smyth D M 1991 *Ferroelectr.* **116** 117-124.
[14] Tan X, Li K 2002 AIChE J. **48** 1469-77.
[15] Anzoletti V 2014 MSc Dissertation in Chemical Engineering, University of L'Aquila.
[16] Di Felice L, Middelkoop V, Anzoletti V, Snijkers F, Van Sint Annaland M, Gallucci F 2014 *Chem. Eng. Process.* doi:10.1016/j.cep.2014.12.004
[17] Rapagnà S, Gallucci K, Di Marcello M, Foscolo P U, Nacken M, Heidenreich S 2009 *Energy Fuels* **23** 3804-3809
[18] Antonini T, Gallucci K, Foscolo P U 2014 *Chem. Eng. Trans.* **37** 91-96.
[19] Di Blasi C 2000 *Chem. Eng. Sci.* **55** 2931-2944
[20] Arthur J R 1950 *Trans. Faraday Soc.* **47** 164-178
[21] Glicksman L R 1984, Heat transfer in fluidized bed combustors, ed P Basu (Toronto: Pergamon Press) 63-100.
[22] Chen J C, Chen K L 1981 *Chem. Eng. Commun.* **9** 255-271.